Microsolvation of the ammonium ion in argon: Infrared spectra of NH_4^+–Arn complexes (n = 1–7)

ARTICLE *in* INTERNATIONAL JOURNAL OF MASS SPECTROMETRY AND ION PROCESSES · NOVEMBER 1997

DOI: 10.1016/S0168-1176(97)00111-0

5 AUTHORS, INCLUDING:

Sergey Nizkorodov
University of California, Irvine
135 PUBLICATIONS **2,843** CITATIONS
SEE PROFILE

Markus Meuwly
University of Basel
180 PUBLICATIONS **2,994** CITATIONS
SEE PROFILE

John P. Maier
University of Basel
517 PUBLICATIONS **8,041** CITATIONS
SEE PROFILE

ELSEVIER International Journal of Mass Spectrometry and Ion Processes 167/168 (1997) 637–647

International Journal of Mass Spectrometry and Ion Processes

Microsolvation of the ammonium ion in argon: infrared spectra of NH_4^+-Ar_n complexes (n = 1–7)[1]

Otto Dopfer*, Sergey A. Nizkorodov, Markus Meuwly, Evan J. Bieske†, John P. Maier

Institut für Physikalische Chemie, Universität Basel, Klingelbergstrasse 80, CH-4056 Basel, Switzerland

Received 25 November 1996; accepted 2 June 1997

Abstract

Infrared spectra of mass selected NH_4^+-Ar_n (n = 1–7) cluster ions have been recorded in the range between 3000 and 3500 cm^{-1} by means of photodissociation spectroscopy. Vibrational assignments are based on ab initio calculations by taking into account complexation-induced frequency shifts and splittings as well as band intensities. The results indicate that the first four Ar atoms occupy equivalent vertex-bound sites, while further Ar atoms are probably located at the faces of the tetrahedral monomer. © 1997 Elsevier Science B.V. © 1997 Elsevier Science B.V.

Keywords: Ab initio studies; Ionic complexes; NH_4^+-Ar_n; Infrared photodissociation spectroscopy; Solvation

1. Introduction

Proton-bound complexes are stabilized intermediates of proton transfer reactions. Their characterization provides useful insight into the dynamics of these reactions which play a key role in many areas of physics, chemistry and biology. In the past, a large amount of information about proton-bound systems has been extracted from mass spectrometric studies by following the properties of mass-selected complexes as they grow in size [1]. Analysis of metastable fractions, fragmentation branching ratios following collisional or photo excitation, and kinetic energy release data provided information on structures and binding energies as a function of cluster size. Solvation shell closure is often indicated by discontinuities in mass spectral abundances (magic numbers) or kinetic energy releases. For example, studies on NH_4^+-$(NH_3)_n$ complexes reveal that the first solvation shell is filled at n = 4 so that the nitrogen atoms of the ligands bind to the vertices of the tetrahedral NH_4^+ core [1–3].

In the last decade, the combination of high resolution laser spectroscopic methods with mass spectrometric techniques has provided direct access to intermolecular interaction potentials of a number of ionic complexes [4,5]. Proton-bound species have been mainly investigated by means of infrared (IR) photofragmentation spectroscopy. Rotationally resolved spectra of dimers have provided detailed information on potential energy surfaces, including equilibrium geometries, bond energies and potential anisotropies [6–11]. Vibrationally resolved spectra have elucidated

* Corresponding author.

[1] Dedicated to Professor Chava Lifshitz on her 60th birthday.

† Present address: School of Chemistry, The University of Melbourne, Parkville, Victoria 3052, Australia.

PII S0168-1176(97)00111-0

Table 1
Experimental and calculated vibrational frequencies (in cm^{-1}) of NH_4^+ (T_d)

Symmetry	ν_1 a_1	ν_2 e	ν_3 t_2	ν_4 t_2	$2\nu_4$ a_1+e+t_2	$\nu_2+\nu_4$ t_2+t_1	$2\nu_2$ a_1+e
Experiment			3343.1[a]	1447.2[b]			
HF[c]	3237	1675	3343	1451			
MP2[d]	3256	1671	3382	1430			
Ab initio force field[e]	3236.6	1690.1	3345.1	1447.2	2860.2 (a_1) 2887.3 (e) 2899.0 (t_2)	3120.5 (t_2) 3138.0 (t_1)	3375.8 (a_1) 3377.1 (e)

[a] Reference [19].
[b] Reference [21].
[c] Harmonic frequencies scaled by a factor of 0.907.
[d] Harmonic frequencies scaled by a factor of 0.951.
[e] Reference [24].

the microsolvation of ions surrounded by several polar and non-polar ligands [6,7,9,12–16]. Geometries and binding energies have been inferred from the analysis of frequency shifts and fragmentation branching ratios, as have the existence of structural isomers and the formation of solvation shells.

The tetrahedral NH_4^+ monomer that acts as the chromophore in the NH_4^+-Ar_n series has been well characterized by both gas phase IR spectroscopy [17–23] and ab initio calculations [24–27]. Two of the four fundamentals, the triply degenerate ν_3 and ν_4 vibrations, are IR active and their frequencies were measured as 3343.1 and 1447.2 cm^{-1}, respectively. A recently calculated high quality ab initio quartic force field [24] reproduces these two fundamentals to within a few wavenumbers and predicts the other two modes to be at 3236.6 cm^{-1} (ν_1) and 1690.1 cm^{-1} (ν_2) (see Table 1).

Until recently, the only NH_4^+-X_n clusters studied using gas phase spectroscopy appear to be the NH_4^+-$(NH_3)_n$ series. Low resolution (25 cm^{-1}) IR absorption spectra for n = 0–4 revealed two NH_4^+ core vibrations between 2000 and 4000 cm^{-1} which were assigned to the strong IR-allowed ν_3 and $2\nu_4$ bands by comparison with earlier ammonium salt crystal data [28]. Higher resolution (~1 cm^{-1}) spectra of mass selected clusters (n = 1–10) obtained by IR vibrational predissociation spectroscopy confirmed the assignment of the spectral features attributed to the ionic core, and showed additional absorptions associated with the NH_3 ligands [12,29]. Complexation-induced frequency shifts as well as symmetry considerations led to the conclusion that the first four ligands form the first solvation shell in agreement with previous thermodynamic data [1] and ab initio calculations [30,31]. Spectral features due to internal rotation of the NH_3 ligands in the first solvation shell vanish for $n > 7$, indicating that each of the second shell ligands forms a hydrogen bond to one first shell ligand. Predissociation spectra in the range of 1045–1091 cm^{-1} for n = 5–8 reveal absorptions that were assigned to collective vibrations associated with the ν_2 modes of the second shell ligands [31].

Recently, the anisotropy of the interaction of NH_4^+ with the rare gas atoms Ar and He has been probed by their ν_3 IR photodissociation spectra [32,33]. Complexation of NH_4^+ with Ar splits the triply degenerate ν_3 vibration into two components: a lower frequency parallel band (a_1) and a higher frequency perpendicular band (e) of a semi-rigid prolate symmetric top with C_{3v} geometry [33]. Analysis of the rotational structure of the latter band revealed that the anisotropy of the potential is relatively large. As a consequence the observed splittings associated with the tunneling motion of the Ar atom between the four equivalent sites of the tetrahedron are small (~1 cm^{-1}).

It was, however, impossible to determine from the spectrum whether the global minimum structure is one where the Ar atom binds to the vertex or to the face of the tetrahedron. In contrast to NH_4^+-Ar, the corresponding ν_3 spectrum of NH_4^+-He closely resembled that of the NH_4^+ monomer, indicating that complexation with He has almost no effect on the vibrational and rotational motions of the NH_4^+ core [32]. Ab initio calculations predict that for this complex the vertex-bound structure ($D_e \sim 147\ cm^{-1}$) is slightly more stable than the face-bound structure ($D_e \sim 130\ cm^{-1}$).

The aim of the present work is to extend the study of the NH_4^+-Ar dimer to larger clusters in order to follow the microsolvation of the ammonium ion in argon. The differences between NH_4^+-Ar_n and NH_4^+-$(NH_3)_n$ complexes can be summarized as follows. (1) Replacing the NH_3 ligands by Ar atoms avoids complications in the spectra due to ligand absorptions. (2) Although the NH_3 molecule is roughly comparable in size to an Ar atom, hydrogen bonding by NH_3 causes a much stronger directionality of the intermolecular bonds in the ligand network. There is a possibility that for the Ar-containing clusters more than four ligands can have close contact to the NH_4^+ core. (3) The binding energy of NH_4^+-Ar ($\sim 500\ cm^{-1}$) is much lower than that of NH_4^+-NH_3 ($\sim 9100\ cm^{-1}$ [30,34]). Thus, the complexation-induced frequency shifts are expected to be significantly smaller. In contrast to NH_4^+-NH_3, the binding energy of NH_4^+-Ar is lower than any intramolecular frequency, i.e. the absorption of a single IR photon is sufficient to dissociate cold cluster ions.

2. Experimental

The experimental approach has been described in detail elsewhere [6,35]. Photofragmentation spectra were recorded in a tandem mass spectrometer coupled to an electron impact cluster ion source. NH_4^+-Ar_n complexes were produced in a pulsed and skimmed supersonic expansion of NH_3, H_2 and Ar with a ratio of about 1:5:100 at backing pressures of 3–5 bar. The cluster size distribution could be shifted to higher n by increasing the Ar concentration and the stagnation pressure. After mass selection by a first quadrupole mass spectrometer, the parent species under investigation, NH_4^+-Ar_n, was irradiated in an octopole ion guide with a counterpropagating IR laser pulse emitted from an optical parametric oscillator system with 0.02 cm^{-1} bandwidth. The energy of the absorbed photon exceeded the binding energy of the intermolecular bonds and eventually led to dissociation of the parent cluster into NH_4^+-Ar_m and $(n - m)$ Ar atoms. A second quadrupole transmitted only fragment ions of a selected size which were subsequently detected by a Daly detector [36]. Photodissociation spectra were obtained by monitoring the fragment ion intensity as a function of the laser frequency. When several fragmentation channels were observed, spectra were recorded for each of them simultaneously by switching the second quadrupole mass filter between the respective fragment masses for each laser wavelength. To compensate for any drift in the background signal, mainly caused by metastable fragmentation of hot parent clusters, the nozzle was triggered at twice the laser frequency, and the 'laser off' signal was subtracted from the 'laser on' signal. Calibration of the laser wavelength was accomplished by comparison with optoacoustic absorptions of NH_3 [37]. All spectra have been corrected for the IR laser power variations measured with an InAs detector. Rotational line positions of the dimer [33] were corrected for the Doppler shift of approximately 0.03 cm^{-1} caused by the kinetic energy of the ions in the octopole of 3 ± 0.5 eV.

3. Ab initio calculations

Ab initio calculations were employed to guide the analysis of the vibrational spectra.

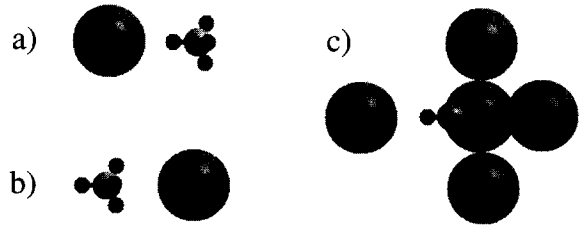

Fig. 1. Sketch of various NH_4^+-Ar_n cluster ion geometries: (a) vertex-bound dimer; (b) face-bound dimer; (c) C_{3v} structure of the $n = 5$ cluster.

Computations at the MP2 level have been carried out to determine the dimer geometry and the influence of the first ligand on the vibrational frequencies of the NH_4^+ monomer. These results were also useful for testing the quality of the results of lower level Hartree–Fock (HF) calculations for the larger clusters (n = 0–5). The Gaussian 94 program package was used throughout [38].

MP2 calculations with contractions (11s,5p,1d) → [4s,3p,1d] on N, (6s,2p,1d) → [3s,2p,1d] on H, and (13s,10p,1d) → [6s,5p,1d] on Ar, equivalent to a VTZ basis with additional polarization and diffuse functions [39], have been employed to calculate geometries and vibrational frequencies of NH_4^+ (100 GTO = primitive Gaussian type orbitals) and NH_4^+-Ar (149 GTO). Two stable minima of the dimer were investigated: the vertex-bound and the face-bound structure (see Fig. 1(a) and (b), respectively). The vertex-bound structure was found to be the global minimum with a binding energy of $D_e \sim 500\ cm^{-1}$ (corrected for basis set superposition error), while the face-bound structure lies $\sim 200\ cm^{-1}$ higher in energy. Harmonic vibrational frequencies of the monomer and both dimer configurations are compiled in Table 2. The most striking difference between the two dimer geometries is the size of the ν_3 band splitting upon complexation. While the calculations predict only a small splitting ($< 1\ cm^{-1}$) for the face-bound structure, a large splitting ($68\ cm^{-1}$) is obtained for the vertex-bound one, in reasonable agreement with the experimental result of $43\ cm^{-1}$. Finally, it is noted that the geometry of the NH_4^+ core is almost unaffected by Ar complexation, in accordance with a relatively weak interaction within the complex.

Larger clusters were investigated only at the HF level. The basis set consisted of the contractions (11s,7p,1d) → [7s,4p,1d] on N, (6s,3p,1d) → [4s,3p,1d] on H, and (13s,10p,3d) → [8s,6p,3d] on Ar, leading to 122, 183, 244, 305, 366 and 427 GTO for n = 0–5, respectively. Harmonic frequencies and complexation-induced frequency shifts calculated for the monomer and the dimer agree qualitatively with those determined on the MP2 level, although as expected quantitative agreement is not obtained, mainly due to the neglect of electron correlation (see Tables 1 and 2). Similar to the MP2 results, the ν_3 band splitting calculated at the HF level is only significant for the vertex-bound dimer; however, its magnitude of $22\ cm^{-1}$ underestimates the experimental splitting of $43\ cm^{-1}$. The binding energies as well as the ν_3 band splittings calculated at both levels of theory lead to the conclusion that the face-bound minima are

Table 2
Calculated harmonic frequencies (in cm^{-1}, unscaled) of NH_4^+ (n = 0) and NH_4^+-Ar (n = 1)[a]

n	Symmetry	Level	ν_1	ν_2	ν_3	ν_4
0	T_d	HF	3569 (a_1)	1847 (e)	3686 (t_2)	1600 (t_2)
1 (vertex)	C_{3v}	HF	3566 (a_1)	1849 (e)	3669 (a_1), 3691 (e)	1597 (a_1), 1604 (e)
1 (face)	C_{3v}	HF	3572 (a_1)	1846 (e)	3691 (a_1), 3689 (e)	1599 (a_1), 1600 (e)
0	T_d	MP2	3424 (a_1)	1757 (e)	3556 (t_2)	1504 (t_2)
1 (vertex)	C_{3v}	MP2	3379 (a_1)	1760 (e)	3495 (a_1), 3563 (e)	1495 (a_1), 1514 (e)
1 (face)	C_{3v}	MP2	3432 (a_1)	1762 (e)	3565 (a_1), 3565 (e)	1507 (a_1), 1510 (e)

[a] For the dimer two stable minima were considered, the face-bound and the vertex-bound configuration.

significantly less stable. Thus, for the larger cluster calculations as well as for the analysis of their experimental spectra, it was assumed that the first four Ar atoms bind to the vertices of the NH_4^+ tetrahedron leading to geometries with T_d, C_{3v}, C_{2v}, C_{3v} and T_d symmetry for $n = 0$–4, respectively. All coordinates were allowed to relax. In clusters with $n > 4$, the additional Ar atoms probably occupy positions at the faces of the tetrahedron. The Ar···Ar separation in the computed NH_4^+-Ar_4 structure of around 6 Å, combined with the vdW radius of Ar (~1.7 Å [40]), suggests that at least one Ar atom can fit within the triangle of three vertex-bound ligands with close contact to the respective face of NH_4^+. It is not clear whether these additional Ar atoms are situated in the centre of the faces leading to geometries with C_{3v}, C_{2v}, C_{3v} and T_d symmetry for $n = 5$–8 [see Fig. 1(c) for $n = 5$], or whether they occupy less symmetric sites, for example in order to maximize the Ar···Ar interaction. Higher level calculations taking electron correlation into account are necessary to analyse the interplay between the various attractive and repulsive forces in these many-body systems in a reliable fashion. In the present work, only the C_{3v} configuration of the $n = 5$ complex was examined by keeping the optimized NH_4^+-Ar_4 geometry frozen and relaxing only the three intermolecular coordinates of the fifth, i.e. the face-bound Ar atom.

4. Results and discussion

4.1. Spectra

Photodissociation spectra of mass-selected NH_4^+-Ar_n complexes recorded in the region between 3000 and 3500 cm^{-1} are reproduced in Fig. 2 for $n = 1$–5. Parts of the low energy region of the spectra are vertically expanded to show the weak features. Possible NH_4^+ monomer fundamentals, overtones and combination bands which fall into the scanned region are indicated by sticks together with their symmetry labels.

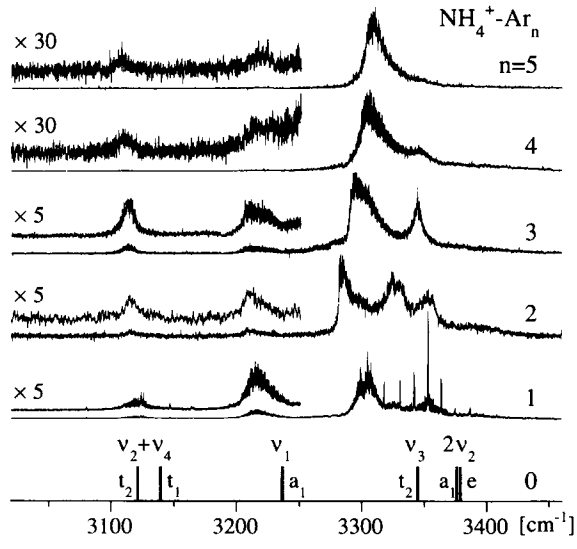

Fig. 2. Photofragmentation spectra of NH_4^+-Ar_n ($n = 1$–5) recorded on the respective dominant fragment channel (see Table 5). Parts of the low energy region of the spectra are vertically expanded to show the weak features. Possible NH_4^+ monomer fundamentals, overtones and combination bands which fall into the scanned region are indicated by sticks together with their symmetry labels.

Their positions have been calculated from the ab initio force field [24] that reproduces the experimental ν_3 and ν_4 frequencies of NH_4^+ to within a few cm^{-1} (Table 1). For $n = 6$ and 7, spectra have been recorded only in the region of the strong bands (3250–3450 cm^{-1}). They are not presented because they are similar in appearance to the spectra for $n = 5$, displaying only a single slightly blue shifted band.

4.2. Vibrational analysis

The assignment of the vibrational spectra was guided by comparison with complexation-induced frequency shifts and splittings predicted by the ab initio calculations. All spectral features observed are attributed to intramolecular vibrations of the NH_4^+ core. Hence, the notation employed for the cluster vibrations refers to the four core vibrations (ν_1–ν_4), and whenever the reduction of the symmetry would split degenerate vibrations into several components, their symmetries are given separately.

Table 3
Comparison of band maxima (in cm^{-1}) for the various components of the ν_3 vibration of NH_4^+-Ar_n with ab initio values

n	Symmetry	Ab initio (HF)[a]	Experiment[b]
0	T_d	3343 (t_2)	3343.1[c]
1	C_{3v}	3327 (a_1)	3305(4)
		3347 (e)	3347.8(1)
2	C_{2v}	3325 (b_2)	3284(3)
		3339 (a_1)	3327(3)
		3351 (b_1)	3354(3)
3	C_{3v}	3331 (e)	3298(4)
		3349 (a_1)	3346(1)
4	T_d	3335 (t_2)	3306(3)
			3347(2)[d]
5	C_{3v}	3336 (a_1)	3310(2)
		3336 (e)	
6			3314(3)
7			3317(2)

[a] Harmonic frequencies scaled by a factor of 0.907.
[b] Positions are measured in spectra recorded on the dominant fragment channel (see Fig. 2 and Table 5).
[c] Reference [19].
[d] Assigned to a less stable isomer.

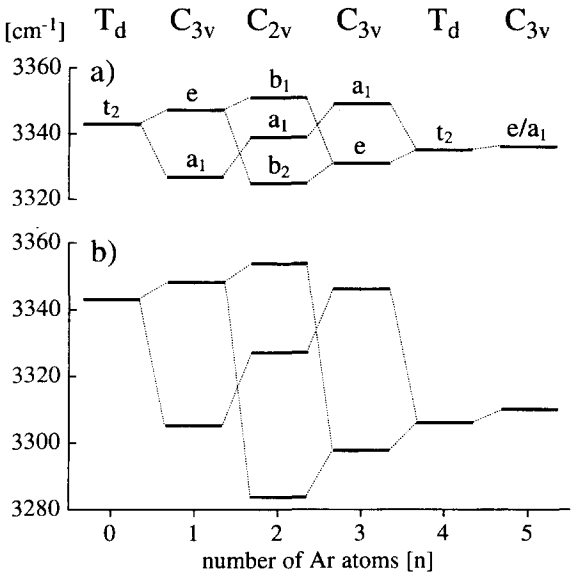

Fig. 3. Theoretical (a) and experimental (b) positions of the various components of the ν_3 vibration of NH_4^+-Ar_n ($n = 0$–5). The ab initio values (HF level) are scaled to match the experimental monomer frequency (see Table 3).

First, the intense bands lying between 3280 and 3400 cm^{-1} are considered. They are assigned to the various components associated with the triply degenerate ν_3 vibration of the NH_4^+ chromophore. The measured band centres are summarized in Table 3 (n = 0–7) along with the theoretical frequencies (HF level, n = 0–5). The latter values were scaled by a factor of 0.907 to match the experimental value for n = 0 (3343 cm^{-1}). Experimental and calculated values are compared graphically for n = 0–5 in Fig. 3. The qualitative agreement of both patterns concerning frequency shifts and splittings prompted an assignment of the symmetries to the various components of the respective ν_3 vibration. Resolution by symmetry reduction of a triply degenerate t_2 vibration in T_d leads to vibrations of symmetry $a_1 + e$ in C_{3v} and $a_1 + b_1 + b_2$ in C_{2v} with all components being IR allowed [41].

For the monomer, the ν_3 origin (t_2/T_d) was determined as 3343 cm^{-1} [19]. In case of the n = 1 complex (C_{3v}), this vibration is resolved into a higher frequency component of e symmetry (perpendicular band) and a lower frequency component of a_1 symmetry (parallel band). A preliminary analysis of the rotational structure of the perpendicular band was presented previously [33]. The vibrational origins were measured as 3305 cm^{-1} (a_1) and 3347.8 cm^{-1} (e), where the latter value was taken as the average of the $K = 0 \leftarrow 1$ and $K = 1 \leftarrow 0$ Q branch positions. The direction of the respective shifts can be rationalized by considering the normal mode components of the triply degenerate ν_3 vibration of a tetrahedral XY_4 molecule [41]. They can be characterized by motions where all four hydrogen atoms vibrate parallel against the central N atom. For a vertex-bound geometry, the a_1 component involves significant stretching of the N–H bond along the N–H–Ar direction, leading to a frequency drop upon complexation. In contrast, the e component involves more bending character of the N–H–Ar bonds, causing the frequency to increase due to the additional angular constraints originating from the intermolecular H–Ar bond. Addition of a second Ar atom leads to a C_{2v} structure and the doubly degenerate

e vibration of the dimer is split further into b_1 and b_2 components, i.e. the three-fold degeneracy of the t_2 monomer vibration is completely removed. For NH_4^+-Ar_3, the structure is again of C_{3v} symmetry consistent with the observation of two strong transitions in the considered spectral range. All four vertices of the ionic core are occupied by Ar ligands for $n = 4$ (T_d) leading to a single band of t_2 symmetry at 3306 cm^{-1}, red shifted by 37 cm^{-1} with respect to the corresponding monomer transition. The direction of the frequency shifts of the $n = 3$ ν_3 components $a_1 + e$ with respect to the $n = 4$ t_2 mode can be explained in a similar way to the corresponding splittings arising when the first ligand is attached to the monomer. Removing the fourth Ar atom leads to an increase in the frequency of the a_1 component compared to the $n = 4$ t_2 band while the e component slightly decreases in frequency.

There is a weak feature slightly shifted to the blue of the $n = 4$ ν_3 band, and its proximity to the $n = 3$ a_1 component suggests that it may be due to another less stable isomer, with three Ar atoms bound to a vertex and a fourth Ar bound to a face of NH_4^+. As mentioned above, Ar atoms located at the face have less influence on the ν_3 transition frequencies compared to vertex-bound Ar atoms. For the face-bound dimer a blue shift without a significant splitting upon complexation has been calculated. A similar behaviour is predicted for the hexamer ($n = 5$) with C_{3v} geometry (see Fig. 3 and Table 3). This is in line with the experimental observation that only a single band is observed in the spectra of $n = 5$–7, indicating that further splittings of the ν_3 band due to symmetry reduction must be small. In addition, while the averaged ν_3 shift for $n = 1$–4 is about 9.4 cm^{-1} per Ar atom to the red, for $n = 5$–7 the transition shifts monotonically back to the blue by about 3.7 cm^{-1} per Ar atom (see Fig. 4), again supporting the model that first the four vertex sites and subsequently the four equivalent face sites are occupied. Unfortunately, it appears that no Ar matrix isolation studies of NH_4^+ have been performed, making it impossible at this stage to compare the cluster bandshifts with the bulk limit.

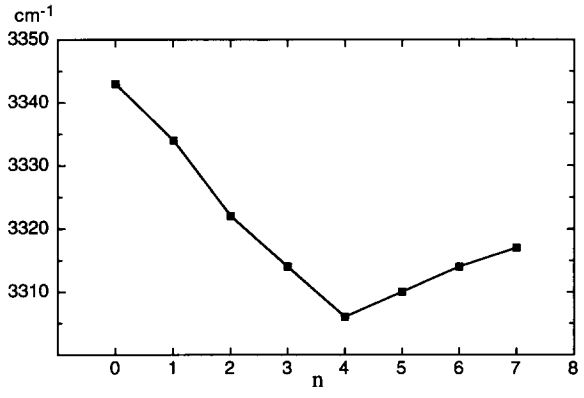

Fig. 4. Averaged position (in cm^{-1}) of the ν_3 vibration of NH_4^+-Ar_n ($n = 0$–7) as a function of cluster size.

The various transitions arising from the overtone of ν_2 also fall in the range of the ν_3 frequency according to theoretical predictions (see Table 1 and Fig. 1); however, they are expected to have much lower intensity than the ν_3 bands. In addition, the agreement between the calculated ν_3 band pattern and the experimental positions of the strong transitions in the 3280–3400 cm^{-1} range (see Fig. 3) make the assignment of these bands to the various ν_3 components almost unambiguous. Very weak and broad features centred around 3390 cm^{-1} in the spectra of n = 2 and 3 may, however, be due to $2\nu_2$ bands (Table 4). This would imply positive complexation shifts of the order of 10–15 cm^{-1} with

Table 4
Further vibrational band positions (in cm^{-1}) for NH_4^+-Ar_n in photofragmentation spectra recorded in the dominant fragment channel

n	ν_1	$\nu_2 + \nu_4$	$2\nu_2$
1	3215(4)	3120(3), 3164.5(1)[a], 3147.1(1)[a], 3080.4(1)[a]	
2	3211(3)	3115(2)	3390(8)
3	3215(4)	3115(2)	3390(8)
4	3217(3)[b]	3111(2)	
5	3220(3)	3107(2)	

[a] Sharp Q branch-like features.
[b] Assigned to a less stable non-tetrahedral isomer.

respect to the predicted monomer transitions at 3375.8 cm^{-1} (a_1) and 3377.1 cm^{-1} (e), compatible with the predicted harmonic ab initio shifts of around 8 cm^{-1} (MP2, Table 2).

We turn our attention now to the weak band series between 3200 and 3250 cm^{-1}. It is associated with the totally symmetric NH stretch mode (ν_1) of NH_4^+ which is of a_1 symmetry in all considered symmetry groups. Thus, it is dipole forbidden for the monomer and the pentamer (T_d), while it becomes weakly allowed for complexes with lower symmetry. This prediction is in close agreement with the experimental observation (Fig. 2), that for n = 1–3 a weak but clearly visible band is present in the expected spectral range, while for n = 4 the relative intensity of the corresponding band drops drastically. The calculations predict for n = 1–3 an intensity ratio of around 0.03–0.1 for ν_1 with respect to the ν_3 components, again in qualitative agreement with the experiment. The fact that the n = 4 band does not vanish completely may again be indicative of less stable isomers with lower symmetry, e.g. one with three Ar atoms bound to vertices and the fourth one bound to a face. For the n = 5 complex, the symmetry is also reduced, turning ν_1 again into an allowed fundamental. However, as expected, the intensity of the observed band is quite weak, indicating that only vertex-bound Ar atoms appreciably distort the symmetric NH stretch mode of the monomer. This observation is supported by the calculations which predict that the ν_1 intensity for the face-bound dimer is about two orders of magnitude lower than for the vertex-bound dimer. In addition, for the C_{3v} hexamer the ν_1 band is calculated to be about three orders of magnitude weaker than the respective ν_3 transitions, again in qualitative agreement with the experiment. Finally, the ν_1 frequency shifts are considered (Table 4). The experimental monomer value is not known, and the probably best theoretical prediction comes from the high level force field calculation [24], ν_1 = 3237 cm^{-1}, with an estimated error of a few wavenumbers. The experimental dimer ν_1 frequency of 3215 cm^{-1} would then imply a red shift of around 20 cm^{-1}. In contrast to the MP2 calculation which predicts a larger shift (45 cm^{-1}), the HF level underestimates it (4 cm^{-1}), which is similar to the ν_3 component shifts. However, the qualitative trend of the ν_1 shift as a function of cluster size can again be reproduced by the HF computations with calculated incremental shifts of −4, −1, +1, +1 and +1 cm^{-1} for n = 1–5, respectively.

The weak transitions in the 3100–3150 cm^{-1} spectral range are attributed to the various components of the $\nu_2 + \nu_4$ combination band. The two monomer transitions are calculated to be at 3120.5 (t_2) and 3138.0 (t_1) cm^{-1} (Table 1). Both the HF and the MP2 calculations predict only small complexation shifts for the ν_2 and ν_4 fundamentals. Symmetry reduction to C_{3v} or C_{2v} resolves the t_1 and t_2 components into various IR allowed symmetry species. For the dimer, a broad feature around 3120 cm^{-1} is observed that is probably due to one or more parallel bands, in addition to several perpendicular type features which could not be definitely assigned. The spectra of the larger clusters show only single broad bands and their positions are given in Table 4. The components of the overtone of the strong IR active ν_4 fundamental are predicted to be near 2900 cm^{-1}; however, an assignment of the discussed bands to these components can be discarded after comparison with the theoretical calculations which predict only small frequency complexation shifts for ν_4. An assignment to a combination of $2\nu_4$ with the IR active intermolecular stretch (ν_S), which could fall into the considered range, also seems unlikely because no combination bands of the strong ν_3 band with ν_S are observed.

With the exception of the e component of the dimer's ν_3 band and the unassigned sharp Q branch-like features near the $\nu_2 + \nu_4$ region, the observed bands do not show resolved rotational structure. The most likely reason for this observation is the finite laser bandwidth of 0.02 cm^{-1}, as may be seen from the dimer's ν_3 band, where

the parallel band is congested due to the overlap of several $\Delta K = 0$ sub-bands, while the perpendicular band could be rotationally resolved in respective P, Q and R branches of separated $\Delta K = \pm 1$ sub-bands. The widths of the unresolved bands vary between 10 and 20 cm^{-1} and may be due to several reasons which cannot be distinguished in the present study. Spectral congestion arising from the overlap of sequence bands of a single isomer and/or bands originating from different structural isomers and/or unresolved splittings caused by symmetry reduction would lead to inhomogeneous broadening. Homogeneous line broadening could be caused by fast dynamical processes such as intracomplex vibrational energy redistribution and/or vibrational predissociation. Small splittings in rotationally resolved dimer bands indicate that the NH_4^+ can undergo hindered internal rotation in the dimer. In order to study the dependence of this internal rotation potential as a function of cluster size, higher resolution spectra are required.

4.3. Photofragmentation ratios and binding energies

Photoexcitation of mass selected NH_4^+-Ar_n complexes in the 3000–3500 cm^{-1} spectral range resulted in narrow distributions of fragment ion sizes. Table 5 summarizes the fragmentation ratios measured for excitation at the respective ν_3 band maxima. For parent complexes with $n < 4$ only molecular NH_4^+ fragment ions were observed. For larger complexes ($n = 4$–7) fragment cluster ions of the form NH_4^+-Ar_m ($m > 0$) were also detected with significant intensity, with the channel corresponding to the loss of four Ar atoms being dominant. In a rough approximation, the averaged binding energy can be estimated by dividing the absorbed photon energy by the number of ligands lost. This simple model gives a binding energy of ~3300/4 = 825 cm^{-1} per Ar atom. The discrepancy between this value and the theoretical prediction of ~500 cm^{-1} may arise from several effects, including the neglect of the initial internal energy of the parent cluster ion and the kinetic and internal energy of the respective fragments in the simple view described above. Unfortunately, efforts to simulate the incremental binding energies in the framework of a more sophisticated statistical model, which was applied to the HCO^+-Ar_n series (n = 1–13) [6], failed because the experimental data set was not sufficient in the present study.

Table 5
Branching ratios for photofragmentation of NH_4^+-Ar_n complexes into the various NH_4^+-Ar_m daughter channels[a]

n	$m = 0$	$m = 1$	$m = 2$	$m = 3$	$m = 4$
1	1.00				
2	1.00				
3	1.00				
4	0.63	0.37			
5		0.68	0.32		
6			0.82	0.18	
7			0.02	0.94	0.04

[a] The ratios were measured for the excitation of the ν_3 vibration at the maxima of the respective band(s). Only contributions larger than 0.01 are listed. The estimated accuracy is ± 0.05.

In cases where two significant fragment channels were observed for a given parent cluster (Table 5) photodissociation spectra were measured for each daughter channel. Fig. 5 shows the respective spectra obtained for $n = 4$ and 5. The spectra obtained for both daughter channels

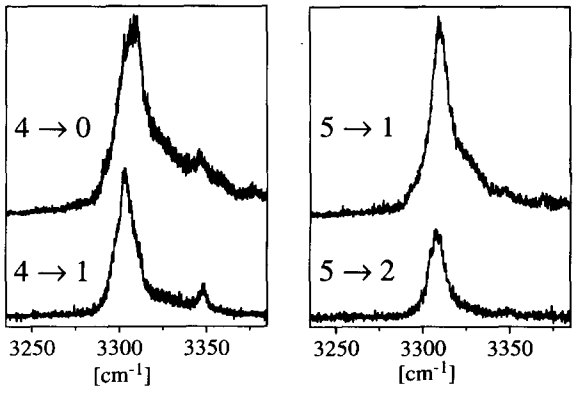

Fig. 5. Photofragmentation spectra of NH_4^+-Ar_n (n = 4, 5) recorded on different fragment channels NH_4^+-Ar_m ($n \rightarrow m$).

are similar in appearance. The bands in the lower mass fragmentation channel are only slightly shifted and broadened compared to the corresponding bands in the larger fragment channel. Similar effects were observed and discussed previously for other weakly proton bound systems, such as for example the HCO^+-Ar_n [6] and the H_3^+-$(H_2)_n$ series [13].

5. Conclusion

The analysis of vibrational bands observed in infrared photofragmentation spectra of mass selected NH_4^+-Ar_n ($n = 1-7$) cluster ions in conjunction with ab initio calculations revealed a consistent picture of the microsolvation process of the ammonium ion surrounded by Ar ligands. The results are in accordance with cluster ion geometries where the first four Ar atoms are located at the vertices of the tetrahedron, while further Ar atoms (up to $n = 8$) occupy equivalent face-bound positions.

Acknowledgements

This study is part of the project no. 20-41768.94 of the Swiss National Science Foundation. Support through the Human Capital and Mobility program 'Structure and Reactivity of Molecular Ions' (BBW grant no. 93.02060) is acknowledged.

References

[1] C. Lifshitz, in: C.Y. Ng, T. Baer, I. Powis (Eds.), Cluster Ions, Wiley, New York, 1993, Chapter 2.
[2] C. Lifshitz, F. Louage, J. Phys. Chem. 93 (1989) 5633.
[3] A.W. Castleman Jr, W.B. Tzeng, S. Wei, S. Morgan, Faraday Trans. 86 (1990) 2417.
[4] C.S. Yeh, J.S. Pilgrim, K.F. Willey, D.L. Robbins, M.A. Duncan, Int. Rev. Phys. Chem. 13 (1994) 231.
[5] T. Buthelezi, D. Bellert, V. Lewis, P.J. Brucat, Chem. Phys. Lett. 242 (1995) 627.
[6] S.A. Nizkorodov, O. Dopfer, T. Ruchti, M. Meuwly, J.P. Maier, E.J. Bieske, J. Phys. Chem. 99 (1995) 17118.
[7] S.A. Nizkorodov, O. Dopfer, M. Meuwly, J.P. Maier, E.J. Bieske, J. Chem. Phys. 105 (1996) 1770.
[8] S.A. Nizkorodov, J.P. Maier, E.J. Bieske, J. Chem. Phys. 103 (1995) 1297.
[9] M. Meuwly, S.A. Nizkorodov, J.P. Maier, E.J. Bieske, J. Chem. Phys. 104 (1996) 3876.
[10] D.W. Boo, Y.T. Lee, J. Chem. Phys. 103 (1995) 514.
[11] D.W. Boo, Y.T. Lee, J. Chem. Phys. 103 (1995) 520.
[12] J.M. Price, M.W. Crofton, Y.T. Lee, J. Phys. Chem. 95 (1991) 2182.
[13] M. Okumura, L.I. Yeh, Y.T. Lee, J. Chem. Phys. 88 (1988) 79.
[14] M. Okumura, L.I. Yeh, J.D. Myers, Y.T. Lee, J. Phys. Chem. 94 (1990) 3416.
[15] J.M. Lisy, in: C.-Y. Ng, T. Baer, I. Powis (Eds.), Cluster Ions, Wiley, New York, 1993, Chapter 4.
[16] M.W. Crofton, J.M. Price, Y.T. Lee, in: H. Haberland (Ed.), Clusters of Atoms and Molecules II, vol. 56, Springer, Berlin, 1994, Chapter 2.3.
[17] M.W. Crofton, T. Oka, J. Chem. Phys. 79 (1983) 3157.
[18] M.W. Crofton, T. Oka, J. Chem. Phys. 86 (1987) 5983.
[19] E. Schäfer, R.J. Saykally, A.G. Robiette, J. Chem. Phys. 80 (1984) 3969.
[20] T. Nakanaga, T. Amano, Can. J. Phys. 64 (1986) 1356.
[21] M. Polak, M. Gruebele, B.W. DeKock, R.J. Saykally, Molecular Phys. 66 (1989) 1193.
[22] E. Schäfer, M.H. Begemann, C.S. Gudeman, R.J. Saykally, J. Chem. Phys. 79 (1983) 3159.
[23] J. Park, C. Xia, S. Selby, S.C. Foster, J. Molecular Spectroscopy 179 (1996) 150.
[24] J.M.L. Martin, T.J. Lee, Chem. Phys. Lett. 258 (1996) 129.
[25] P. Botschwina, J. Chem. Phys. 87 (1987) 1453.
[26] Y. Yamaguchi, H.F. Schäfer III, J. Chem. Phys. 73 (1980) 2310.
[27] D.J. DeFrees, A.D. McLean, J. Chem. Phys. 82 (1985) 333.
[28] H.A. Schwarz, J. Chem. Phys. 72 (1980) 284.
[29] J.M. Price, M.W. Crofton, Y.T. Lee, J. Chem. Phys. 91 (1989) 2749.
[30] K. Hirao, T. Fujikawa, H. Konishi, S. Yamabe, Chem. Phys. Lett. 104 (1984) 184.
[31] M. Ichihashi, J. Yamabe, K. Murai, S. Nonose, K. Hirao, T. Kondow, J. Phys. Chem. 100 (1996) 10050.
[32] O. Dopfer, S.A. Nizkorodov, M. Meuwly, E.J. Bieske, J.P. Maier, Chem. Phys. Lett. 260 (1996) 545.
[33] E.J. Bieske, S.A. Nizkorodov, O. Dopfer, J.P. Maier, R.J. Stickland, B.J. Cotterell, B.J. Howard, Chem. Phys. Lett. 250 (1996) 266.
[34] A.T. Pudzianowsky, J. Chem. Phys. 102 (1995) 8029.
[35] E.J. Bieske, Faraday Trans. 91 (1995) 1.
[36] N.R. Daly, Rev. Sci. Instrum. 31 (1960) 264.
[37] G. Guelachvili, K.N. Rao, Handbook of Infrared Standards, Academic, London, 1993.
[38] M.J. Frisch, G.W. Trucks, H.B. Schlegel, P.M.W. Gill, B.G. Johnson, M.A. Robb, J.R. Cheeseman, T. Keith, G.A. Petersson, J.A. Montgomery, K. Raghavachari, M.A. Al-Laham,

V.G. Zakrzewski, J.V. Ortiz, J.B. Foresman, J. Cioslowski, B.B. Stefanov, A. Nanayakkara, M. Challacombe, C.Y. Peng, P.Y. Ayala, W. Chen, M.W. Wong, J.L. Andres, E.S. Replogle, R. Gomperts, R.L. Martin, D.J. Fox, J.S. Binkley, D.J. Defrees, J. Baker, J.P. Stewart, M. Head-Gordon, C. Gonzales, J.A. Pople, Gaussian, Inc, Pittsburgh, PA, 1995.

[39] Extensible Computational Chemistry Environmental Basis Set Database, version 10, 1996.

[40] J.M. Hutson, Annual Rev. Phys. Chem. 41 (1990) 123.

[41] G. Herzberg, Molecular Spectra and Molecular Structure. II. Infrared and Raman Spectra of Polyatomic Molecules, Krieger, Malabar, 1991.